Seafloor Habitat Mapping by Combining Multiple Features From Optic and Acoustic Data: A Case Study From Ganquan Island, South China Sea

Jiaxin Wan, Zhiliang Qin, Xiaodong Cui, Muhammad Yasir, and Benjun Ma

***Abstract*—Seafloor habitat mapping plays an important role in marine environment monitoring and marine geological research. Optic and acoustic remote sensing are becoming common survey tools in seafloor habitat mapping. However, a single acoustic or optic technique may have a limited detection range and be more susceptible to the impact of image quality. Additionally, it is challenging to satisfy the requirements for accurate detection since single-source data cannot fully reflect the substrate distribution characteristics. This article developed a method for detecting coastal seafloor habitats through the fusion of multiscale optics and acoustics data. First, the original feature set was composed of multispectral satellite data and bathymetric data by multibeam echo sounder and airborne light detection and ranging at different scales, which improved the capacity to represent feature information. Then, a ReliefF–mRMR method was implemented to select optimal features with appropriate scales and remove redundant features. Finally, the optimal features were employed in model training and classification of several supervised classifiers to verify the effectiveness of the strategy. The developed method was applied to the Ganquan Island survey in the South China Sea. The results demonstrated that, after integrating multisource data, the accuracies were up to 3.31% and 17.28% higher than those obtained using multispectral data or bathymetric data alone, respectively. ReliefF–mRMR exhibited better performance than other feature selection methods. The average coral coverage in the study area was estimated to range from 70.85% to 80.33%. This research highlights the greater potential of multisource data for precisely detecting seafloor habitats.**

***Index Terms*—Multiscale features, multisource data fusion, reliefF–mRMR, seafloor habitat mapping.**

Manuscript received 27 April 2023; revised 12 June 2023 and 8 July 2023; accepted 19 July 2023. Date of publication 24 July 2023; date of current version 9 August 2023. This work was supported in part by the National Natural Science Foundation of China under Grant 41876053, Grant 42006064, and Grant 52201400, and in part by Shandong Provincial Natural Science Foundation under Grant ZR2022QD043. *(Corresponding author: Zhiliang Qin.)*

Jiaxin Wan, Zhiliang Qin, and Benjun Ma are with the Acoustic Science and Technology Laboratory, Harbin Engineering University, Harbin 150001, China, and with the Key Laboratory of Marine Information Acquisition and Security (Harbin Engineering University), Ministry of Industry and Information Technology, Harbin 150001, China, and also with the College of Underwater Acoustic Engineering, Harbin Engineering University, Harbin 150001, China (e-mail: wanjiaxin0826@hrbeu.edu.cn; qinzhiliang@hrbeu.edu.cn; mabenjun@hrbeu.edu.cn).

Xiaodong Cui is with the College of Geodesy and Geomatics, Shandong University of Science and Technology, Qingdao 266590, China (e-mail: xiaodong6777@126.com).

Muhammad Yasir is with the College of Oceanography and Space Informatics, China University of Petroleum (East China), Qingdao 266580, China (e-mail: ls1801004@s.upc.edu.cn).

Digital Object Identifier 10.1109/JSTARS.2023.3298472

I. Introduction

SEABED sediment is an important part of geomorphology, and bottom sediment classification is an important tool for understanding the distribution of sediments. Since different seafloor organisms prefer different seafloor geomorphologies for foraging, spawning, and avoiding natural enemies, there is a strong correlation between sediment classification and seafloor habitats [1]. Seafloor habitat mapping is crucial for seabed biotic and abiotic resource assessment, marine space management, and support of marine protected areas and fisheries reserves [2], [3]. Conventional in situ sampling approaches were initially used to quantify benthic habitats while investigating the seafloor surface. Still, they have disadvantages, such as low efficiency, high subjectivity, and limited sampling, particularly in deep waters [4]. To date, the exploration devices for seafloor habitat mapping are basically mature, and the mainstream has developed into optical and acoustical sensors.

The optical remote sensing techniques for seafloor habitat mapping mainly include active airborne light detection and ranging (LiDAR) and passive satellite sensors [5], [6], [7]. Through waveform processing, airborne LiDAR can differentiate several types of seafloor from bottom returns and measure the depth of shallow-water regions. Optical satellite remote sensing offers a cost-effective alternative and has the potential for broad spatial coverage and high temporal resolution [8]. However, owing to the significant attenuation of optical signals in the water, airborne LiDAR and optical satellites can only detect the seabed in very shallow and clear waters, and the image quality decreases significantly with increasing water depth.

The acoustic signal has minimal attenuation in water, making acoustic transmission the most appropriate mechanism for transmitting information through the water column [9], [10]. Shipboard multibeam echo sounder (MBES) is rapidly becoming the most common acoustic survey tool of choice [11], [12], mainly because it allows the collection of continuous bathymetric information. High-resolution and high-precision bathymetric information is of key importance in characterizing substrate types. Numerous studies have experimentally revealed that bathymetric derivatives are highly correlated with the distribution of substrates (e.g., with steep ridges, crests, and depressions being dominated by rock and wide, flat plains being located in sand-dominated areas of bays) [13], [14]. Koop exclusively used multiple bathymetric derivatives to classify substrates in

parts of Norwegian waters [15]. However, shipboard MBES data collection is costly and highly challenging in very shallow water [16]. In addition, MBES images tend to contain stripes and noise.

In short, single-source data yield images with noise and have limited coverage. Besides, in nearshore coastal areas, there are various types of seafloor substrates with a mixed sedimentation phenomenon. All these factors make it difficult to reflect the attributes and distribution characteristics of seabed substrates with only one data source. The combination of multisource data can compensate for the limitations of single-source data and achieve high-precision, full-coverage substrate classification. Some studies have demonstrated the advantages of combining multisource data to map seabed substrates and habitats [14], [17], [18], [19]. Wang et al. [20] merged multibeam backscatter and airborne LiDAR data and found that joint classification achieved comparatively higher accuracies than single-source classification, although accuracy evaluation was conducted in only a small part of the study area. Zhang et al. [21] investigated the terrain complexity parameter and mapped seabed coral abundance using LiDAR and multibeam bathymetry data without considering classification accuracy. Presently, benthic surveying of the seafloor via the combination of acoustics and optics is still in its infancy, as evidenced by the few relevant experiments and insufficient accuracy assessments. Therefore, assessing the effectiveness of the method requires more experimental validation. In addition, although accompanied by more extractable features, habitat mapping studies using multisource data seldom employ feature selection methods, so their feature set is not necessarily a good representation of the differences in each class.

In the context of the acquisition and fusion of multisource information, the features used for detection and classification exhibit scale complexity and dimensional explosion. On the one hand, different scales can fully reflect the characteristics of different classes and their topographic distributions. Therefore, it is necessary to extract multiscale features [22]. On the other hand, a larger feature set often leads to an increase in redundant and low-quality features, which may negatively impact classification, particularly for seafloor surveys with insufficient ground truth data [23], [24]. Therefore, optimizing and selecting high-dimensional feature sets formed by multisource and multiscale features is a key challenge. In recent years, a variety of feature selection methods have been employed to select a subset of features for the purpose of creating simpler and more reliable learning models [24], [25], [26]. Cui et al. [24] proposed a seabed sediment classification model using the deep belief network based on fuzzy ranking feature optimization. Ji et al. [25] utilized the selecting optimal random forest (RF) model to acquire the importance of each feature and determined the feature dimension according to certain decision principles. Although both classification models based on feature optimization significantly improved the accuracy compared with the original feature set, these methods have high computational complexity or poor universality. Relevant studies have focused only on the selection of acoustic features with a single scale, and more analysis and assessment of multisource and multiscale features are needed.

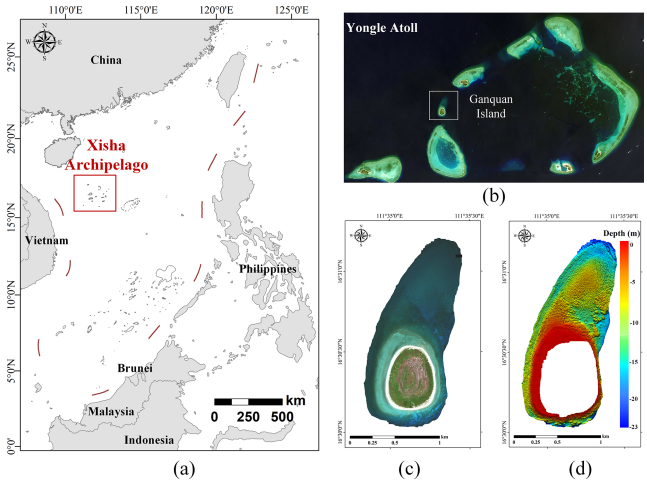

Fig. 1. Study area. (a) Location of Xisha Archipelago. (b) Location, (b) multispectral remote sensing image, and (c) bathymetric data of Ganquan Island.

The objectives of this research mainly include three aspects.

1) To extract features reflecting substrate differences accurately based on multisource fusion techniques.
2) To mitigate the impacts of feature spatial-scale differences and interference features for the classification task.
3) To accomplish continuous high-resolution detection of coastal seafloor habitats.

To achieve these objectives, this paper proposes, develops and tests a classification approach that combines optic and acoustic remote sensing features to produce high precision seafloor habitat maps in Ganquan Island, Xisha Archipelago. We first extract multispectral data (obtained by GeoEye 1 satellite) and bathymetric features (obtained by MBES and LiDAR) of different scales. A ReliefF mRMR strategy is then de veloped to select optimal features with the most appropriate scales and remove redundant features. Finally, four supervised classification models are constructed to achieve the prediction of sand, coral reef, reef crest, and coral fragments and gravel, and the classification results are compared with those of traditional methods.

The rest of this paper is organized as follows. Section II presents the study sites and experimental data. Section III introduces the proposed method. Section IV reports experimental results. Section V provides further discussion on the basis of Section IV. Finally, Section VI concludes the article.

II. Study Sites and Experimental Data

The study site is located on Ganquan Island, Xisha Archipelago, South China Sea (see Fig. 1). The land has an area of approximately 0.3 km^2 and belongs to the temperate marine climate. The bathymetry of the study area ranges from 0 to −23 m. Water depth increases from the land in the southern area to the reef flat in the north. A significant number of coral reefs have developed on the high platform close to the shore because of the relatively stable surface temperature of its water. The ecosystem of the local coral reefs has been harmed in recent years due to increased human activity, and the environmental conservation and habitat investigation are gradually gaining

TABLE I
PARAMETERS OF SENSORS AND MEASUREMENTS

Sensor	Parameter	Index
GeoEye-1	Number of bands	4
	Swath width	15.2 km
	Revisit time	<3 days
	Spatial resolution	0.41 m (Panchromatic) 1.64 m (Multispectral)
WorldView-2	Number of bands	8
	Swath width	16.4 km
	Revisit time	1.1 days
	Spatial resolution	0.46 m (Panchromatic) 1.80 m (Multispectral)
MBES	Acquisition date	2016
	Data collection	R2SONIC 2024
	Data processing	CARIS HISP/SISP 9.1 package
	Tide measurement	AML tidal gauge
	Sound velocity measurement	CTD logger (Ocean Seven304)

greater attention. This region is dominated by coral habitats, including rocks, reefs, and sand. Because of its heterogeneous substrate distribution, this region is ideal for evaluating the efficacy of various approaches for classifying seafloor habitats [20], [27].

A GeoEye-1 image acquired on February 18, 2013, was used as the remote sensing data for mapping the habitats on Ganquan Island. The GeoEye-1 satellite has a high spatial resolution of 0.41 m (pan) and 1.61 m (multispectral). The multispectral image has four bands: blue (450–510 nm), green (520–580 nm), red (655–690 nm), and near infrared (780–920 nm). The image was acquired when the cloud cover was less than 10%. As a part of the preprocessing stage, geometric and atmospheric corrections were applied to the raw image.

The bathymetric data were mainly collected in May 2016 by a high-resolution shallow-water MBES, R2SONIC 2024, and processed by the CARIS HISP/SISP 9.1 package [21]. The swath sector in real time for R2SONIC 2024 is 10°–160°, and its frequency ranges from 200 to 400 kHz. To ensure the horizontal coverage rate, the spacing between adjacent survey lines was adjusted according to the depth to achieve different overlap rates of 40%–70%. The parameters of the sensors and measurements are listed in Table I.

In very shallow water, ships could not safely approach the nearshore waters of Ganquan Island, so no MBES data were available for these regions; only a single-beam echo sounder installed on a dinghy could take isolated depth measurements. Bathymetric data acquired using airborne LiDAR were required as a supplement to provide complete and seamless coverage of the seafloor habitats. After manually removing outliers, all bathymetric data were gridded into *XYZ* format with a 2-m horizontal resolution. Field data were obtained by diving, underwater photography, and video recording. Owing to the different

TABLE II
NUMBER OF TRAINING AND TEST SAMPLES IN GANQUAN ISLAND

Class name	Training	Test
Sand	148	120
Coral reef	276	242
Reef crest	112	104
Coral fragments and gravel	76	78
Total	612	544

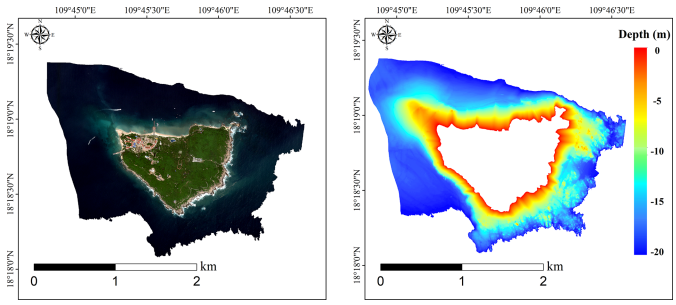

(a) (b)

Fig. 2. Multispectral and bathymetric data of Wuzhizhou Island. (a) World View-2 multispectral image. (b) Bathymetric image.

TABLE III
NUMBER OF TRAINING AND TEST SAMPLES IN WUZHIZHOU ISLAND

Class name	Training	Test
Sand	582	400
Coral reef	583	455
Coral fragments and gravel	201	143
Total	1366	998

proportions of different classes in the study area, unbalanced sample datasets were selected, with 612 training samples and 544 test samples (see Table II). To ensure the representativeness of the samples, the training and test samples were manually selected in different regions of the study area.

To further verify the universality of our proposed method, we also conducted research on Wuzhizhou Island, Hainan province (see Fig. 2). The island has several naturally formed bays and beaches, and the visibility of the sea around the island is high. The multispectral image was obtained by the WorldView-2 satellite in September 2012. The WorldView-2 image includes four standard bands (red, green, blue, and near infrared) and four additional bands (coastal blue, yellow, red edge, and near infrared II). The bathymetric data were also collected by the R2SONIC 2024 MBES in 2016, ranging from 0 to 20 m. The preprocessing method was consistent with that of Ganquan Island, as shown in Table I. In this area, we selected 1366 training and 998 test samples (see Table III). The specific application of this data is shown in Section V.

III. METHODOLOGY

We propose a novel seafloor habitat mapping method that combines optic and acoustic remote sensing data. This method mainly includes three steps.

1) First, we extract multiscale features from the multispectral image and bathymetric data, where the fusion of acoustic and optic information can compensate for the limited detection range and incomplete representation of the substrates by single-source data. Additionally, multiscale characteristics can understand the process of interest more thoroughly.
2) To select the most appropriate scale of different features, remove redundant and irrelevant features, and reduce data dimensionality, we propose ReliefF–mRMR for feature selection.
3) Based on the selected features, four popular supervised machine learning classifiers are then employed to verify the feasibility of our proposed method. The research framework is shown in Fig. 3.

A. Multiscale Feature Extraction

Using default scales alone may not be appropriate for representing the processes of interest [28], [29]. Previous studies have illustrated that the results and interpretation can be impacted by different scales in the marine environment [30], [31]. In addition, since different habitats vary in size and scale, a single scale of features may ignore some details or macroscopic differences between classes. We extract multiscale features from the multispectral image and the bathymetry grid by calculating the original data map using sliding windows of different sizes [32]. The scales of different features are determined by the range of the study area, the resolution of the data, and the feature diversity.

For the multispectral image, we extract the band derivatives, band math features, and texture features to comprehensively represent the global and local statistics. The gray-level co-occurrence matrix (GLCM) is commonly used when describing surface textures [33]. Moreover, many bathymetric derivatives are calculated from bathymetric data, such as slope, aspect, and the bathymetric position index (BPI). The bathymetric derivatives represent the macro- and microtopography of the seafloor, including the structural and scattering properties. The GLCM of water depth is not calculated since relevant studies rarely use this feature, and bathymetric derivatives, in a sense, represent the variations in topographic textures [24], [34]. Details of the feature variables are shown in Tables IV and V.

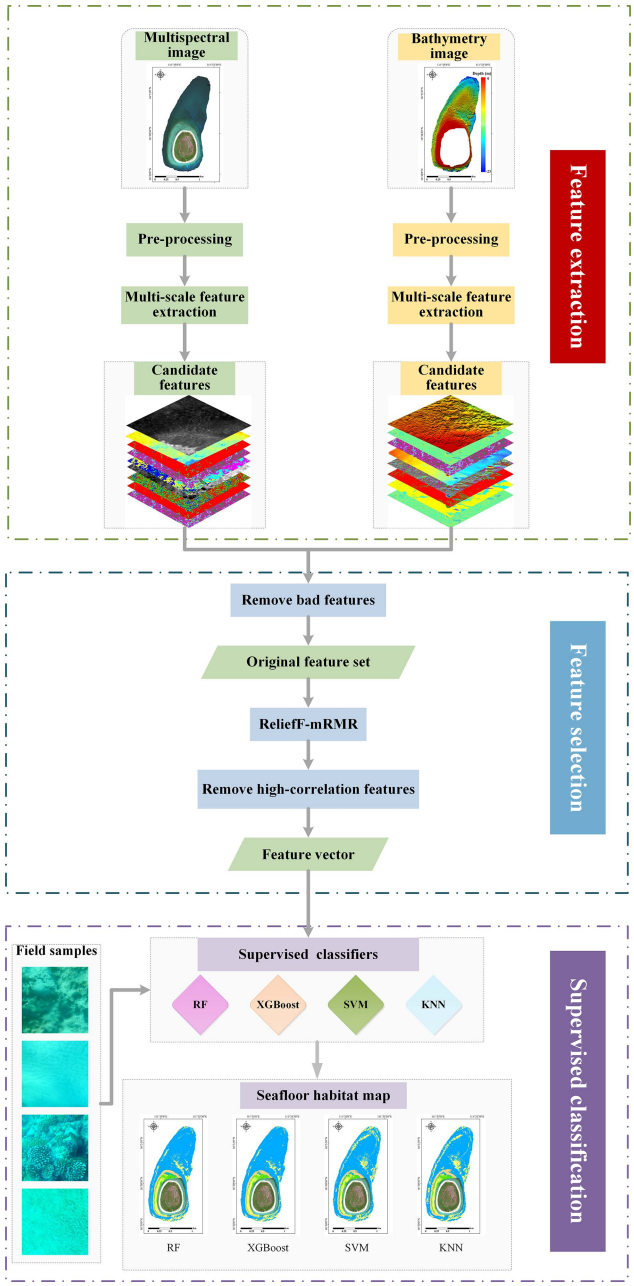

Fig. 3. Research framework.

B. ReliefF–mRMR Feature Selection Algorithm

After extracting multiscale features from the optics and acoustics data, poor features, i.e., those with a messy distribution or less useful information, are identified and removed by manual selection. After this process, 158 features are available as candidates. For small samples, the prediction ability may decrease as the feature dimensionality grows with a fixed number of training samples [36]. In this article, we propose a robust filter-based feature selection model, ReliefF–mRMR, because of the complex scale of benthic habitats and the tendency for mixed deposition. ReliefF–mRMR not only offers different weights to different features to obtain the most appropriate scales of features but also minimizes the redundancy between features and reduces the computational effort. ReliefF–mRMR combines the benefits of the ReliefF and mRMR algorithms.

The ReliefF algorithm is able to assign higher weights to features with good classification capacity [37]. However, not accounting for the redundancy between features may result in no significant improvement in classification accuracy after feature selection, especially unreliable with insufficient training samples [38]. The mRMR algorithm can extract features with minimum redundancy and maximum correlation between features and classes. However, the mRMR algorithm has high computational expense and complexity; the extracted feature set cannot accurately reflect the discrepancies in the roles of

TABLE IV
DETAILS OF THE EXTRACTED FEATURES OF THE MULTISPECTRAL IMAGE

Feature	Explanation	Scale(m)
Band	Electromagnetic bands with frequencies in a certain range	-
Derivatives of bands	Differential coefficient of absorption spectrum with respect to wavelength	-
The second derivatives of bands	Second-order differential coefficient of absorption spectrum with respect to wavelength	-
Normalized difference ratios	The formula is (a−b)/(a+b), where a and b denote the different bands	-
Band ratio	The formula is a/b, where a and b denote the different bands	-
Texture based on co-occurrence matrix	The co-occurrence matrix is a function of both the angular relationship and distance between two neighboring pixels [33].	3,7,11,15, 19,23

*"-" in the column of "Scale(m)" means these features are irrelevant to the calculation scales.

TABLE V
DETAILS OF EXTRACTED BATHYMETRIC DERIVATIVES

Feature	Explanation	Scale(m)
Depth	Negative elevation of the grid.	-
Aspect	Deviation of aspect from 0. Description of the orientation of the slope.	5,15,25,35,45
Slope	Maximum rate of change in depth between each cell and its analysis neighborhood (degrees from horizontal) [22].	5,15,25,35,45
RDMV	A measure of relative position. It can help identify peaks and pits. $rdmv = (local\ mean - initial\ depth\ value) / (local\ range)$	5,15,25,35,45
Eastness	The sine of the aspect in radians. This is a component of the aspect that provides information about the slope's orientation.	5,15,25,35,45
Northernness	The cosine of the aspect in radians. This is the second component of the aspect that provides information about the slope's orientation.	5,15,25,35,45
Standard Deviation	A measure of rugosity/ruggedness/roughness.	5,15,25,35,45
Local mean	Correlated with other statistical terrain attributes (e.g. median, maximum, and minimum).	5,15,25,35,45
Ruggedness	Calculated by comparing the absolute values of the differences between the core pixel and its neighbors [35].	5,15,25,35,45
Roughness	The discrepancy between the minimum and maximum bathymetry of a cell and its eight neighbors [35].	5,15,25,35,45
Broad_BPI Fine_BPI	The vertical difference between a cell and the mean of the local neighborhood [26]. The minimum Broad BPI and Fine BPI are calculated using 25/100 m and 5/25 m radius, respectively.	5,15,25,35,45

* "-" in the column of "Scale(m)" means these features are irrelevant to the calculation scales.

various features for classification due to the absence of weights [39], which may lead to the mistaken removal of features that are beneficial for discrimination. Therefore, ReliefF–mRMR is employed, which combines the advantages of ReliefF and mRMR. To obtain the candidate feature sets with high relevance to each habitat, the ReliefF algorithm is utilized to reserve valuable features while minimizing the computational expense of the mRMR algorithm. The mRMR algorithm is then employed to remove the redundant features among the candidate features. Table VI presents the details of the ReliefF–mRMR feature selection algorithm.

In addition, we introduce the classical feature selection method—principal component analysis (PCA)—which preserves more than 85% of the information in the bands. We also employ fuzzy ranking (FR) and the variance inflation factor (VIF), which have been proposed for feature optimization in seabed substrate mapping in recent years [25], [55]. These feature selection methods are used and compared to verify the effectiveness of the ReliefF–mRMR algorithm.

C. Classification Methods and Accuracy Assessment

This study uses four popular machine learning classifiers to map the habitat based on the multiscale features derived from optics and acoustics data, as described in the following text.

1) Random Forest: RF assembles multiple classification decision trees [40]. The final classification result is determined based on the voting results of each tree. Compared with a single decision tree, RF is less sensitive to the overfitting and quality of training samples [41] and is more stable and generalizable. Recent years have seen a rise in the popularity of RF, which has consistently performed well in seabed mapping [42].

2) Extreme Gradient Boosting (XGBoost): XGBoost is an improvement of the gradient boosting decision tree [43]. The main idea of the gradient boosting algorithm is that each model update is in the negative direction of the gradient from the previous round of the loss function. Decision tree algorithms, such as XGBoost and RF, are better suited for this scenario than neural networks because of the small size of the experimental dataset. Wang et al. [44] found that both XGBoost and RF

TABLE VI
DETAILED DESCRIPTION OF THE RELIEFF–MRMR FEATURE SELECTION ALGORITHM

ReliefF–mRMR Feature Selection Algorithm

Input: 1) The original feature set
2) T field samples with labels

Step 1: The weight of the l^{th} feature variable is defined as follows:

$$w_l = \frac{1}{2}\sum_{t=1}^{T} d(x_{l,t}, x_{M_{l,t}}) - d(x_{l,t}, x_{H_{l,t}}), \quad (1)$$

where $x_{l,t}$ is the value of the instance X_t on the l^{th} feature dimension. $x_{H_{l,t}}$ and $x_{M_{l,t}}$ denote the values on the l^{th} feature of the nearest points to X_t with the same class label, and the different class label respectively. $d(\cdot)$ means the calculation of a distance measurement.

The m features with weights larger than the threshold ε_1 are saved.

Step 2: Calculating $\max(D-R)$ based on the m features. Keeping the n features with the largest value.

$$R = \frac{1}{|\boldsymbol{S}|^2}\sum_{x_i, x_j \in \boldsymbol{S}} I(x_i, x_j) \quad (2)$$

$$D = \frac{1}{|\boldsymbol{S}|}\sum_{x_i \in \boldsymbol{S}} I(x_i, z) \quad (3)$$

where $\boldsymbol{S}$ is the feature set, $|\boldsymbol{S}|$ is the number of samples of this feature, x_i and x_j are the feature variables, and z is the target class. $I(x, y)$ is the mutual information between features in the feature subset as well as between features and classes

$$I(x,y) = \iint p(x,y)\log\frac{p(x,y)}{p(x)p(y)}dxdy \quad (4)$$

Step 3: Calculating the correlation coefficients $\hat{r}$ of the n features. The features with the largest $|\hat{r}|$ are removed to get the final feature set.

Step 4: Recalculating the weight of each feature.

Output: A new feature set with weights for each variable.

showed good classification performance in mapping seafloor habitats.

3) Support Vector Machine (SVM): Its decision boundary is the maximum-margin hyperplane solved for the samples [45]. By using kernel functions to transform high-dimensional feature data, SVM can address the problem that classes cannot be separated linearly [46], but it is greatly influenced by the kernels and parameters. In previous studies on seabed mapping, SVM was always inferior to RF [47], [48], [49]. In this experiment, the SVM classifier with the RBF kernel is applied since the RBF kernel often performs better than the other kernels [27], [47].

TABLE VII
PARAMETER SETTING OF DIFFERENT CLASSIFIERS

Classifier	Parameter
RF	*MinLeafSize=1* *number of trees=100*
XGBoost	*n_estimators=1000* *max_depth=6* *min_child_weight=1* *loss function: softmax*
SVM	*kernel_type: radial basis function* *gamma in kernel function: 0.5*
KNN	*NumNeighbors=3* *Distance metrics: Euclidean*

4) K-Nearest Neighbor (KNN): KNN examines the K samples most similar to the samples to be classified, which is determined by the distance between the test and training samples [50]. The choice of the K value is crucial. If the K value is too small, it cannot fully represent the characteristics of the samples; when the K value is too large, training instances that are distant from the input instance can also play a role in the prediction, which affects classification accuracy. KNN has been applied to many substrate classification studies [34].

5) Parameter Setting: The optimal parameters of the aforementioned four classifiers are adjusted by fivefold cross validation. The detailed parameters of these models are shown in Table VII.

6) Accuracy Assessment: In the experiments, the user's accuracy (UA), producer's accuracy (PA), overall accuracy (OA), and Kappa coefficient are used to represent the prediction accuracy [51], [52]. We also introduce a weighted average of precision and recall, and the $F1$-score to show the classification capacities of classifiers, which is a reliable measurement when datasets are imbalanced [53].

IV. RESULTS AND ANALYSIS

A. Feature Selection Results

After selecting the most relevant features and removal of the redundant features by ReliefF–mRMR, 20 predictor variables are obtained. Next, the number of predictor variables is reduced to 16 by correlation analysis, retaining eight multispectral features and eight bathymetric derivatives (see Figs. 4 and 5). Most bathymetric derivatives may be able to better reflect seafloor habitat characteristics at a scale of 15. The weights of different features are shown in Fig. 6. The proportions of bathymetric and multispectral features are comparable, indicating that single-source data are important for classification. Eastness (15) has the largest percentage at 21.1%.

B. Experimental Results of Different Classification Methods

Based on the selected multiscale optic and acoustic features, four typical classifiers are used to construct the seafloor habitat classification models and conduct the accuracy assessment. This section compares and analyzes the classification results of different data sources and feature selection methods.

TABLE VIII
MODEL EVALUATION RESULTS WITH DIFFERENT INPUTS

Model	Feature combination	Sand		Coral reef		Reef crest		Coral fragments and gravel		OA (%)	Kappa	*F*1-score
		UA (%)	PA (%)	UA (%)	PA (%)	UA (%)	PA (%)	UA (%)	PA (%)			
RF	Input1	83.73	95.83	96.00	89.26	90.99	97.12	95.65	84.62	91.54	0.880	0.916
	Input2	59.13	56.67	86.92	93.39	92.45	94.23	74.60	60.26	80.70	0.719	0.802
	Input3	92.00	95.83	97.47	95.46	92.66	97.12	95.83	88.46	**94.85**	**0.926**	**0.948**
XGBoost	Input1	86.89	88.33	93.42	93.80	97.12	97.12	96.00	92.31	93.02	0.900	0.930
	Input2	58.02	63.33	80.93	85.95	90.65	93.27	67.35	42.31	76.10	0.652	0.755
	Input3	95.92	78.33	90.04	97.11	94.55	100.00	100.00	96.15	93.38	0.904	0.932
SVM	Input1	78.10	89.17	91.40	83.47	83.20	100.00	100.00	78.21	87.13	0.817	0.871
	Input2	59.79	48.33	76.43	83.06	82.26	98.08	98.33	75.65	77.21	0.668	0.766
	Input3	77.86	90.83	93.78	87.19	89.66	100.00	100.00	80.77	89.52	0.851	0.896
KNN	Input1	71.43	91.67	95.33	84.30	85.95	100.00	100.00	70.51	86.95	0.815	0.871
	Input2	57.04	64.17	80.81	90.50	85.42	78.85	95.24	51.28	76.84	0.659	0.765
	Input3	76.22	90.83	95.09	88.02	85.95	100.00	100.00	71.80	88.60	0.838	0.886

*Input1, Input2 and Input3 represent the multispectral data only, bathymetric data only, and multisource data, respectively. The bold numbers represent the highest accuracy in the same column.

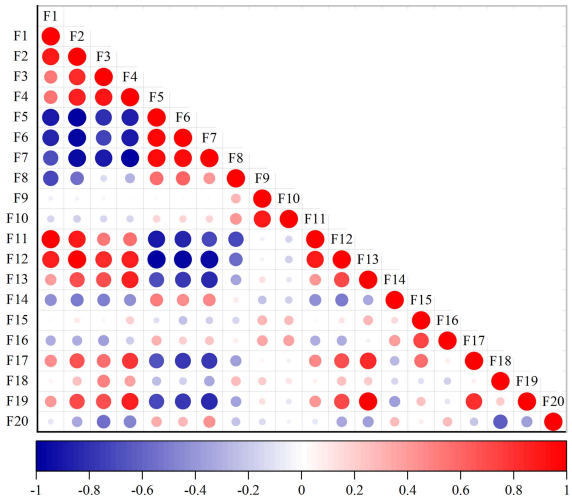

Fig. 4. Correlation analysis between different features. F1–F20 represent the 20 features selected by ReliefF–mRMR. F1–F3: Band 1 (B1)–Band 3 (B3), F4: B1 derivative, F5: B3 derivative, F6: B1 second derivative, F7: B2 second derivative, F8: B1 homogeneity (19), F9: B2 correlation (19), F10: B2 correlation (15), F11: B2 correlation (11), F12: B2 mean (3), F13: Depth, F14: Ruggedness (15), F15: Fine_BPI (25), F16: Fine_BPI (15), F17: Broad_BPI (15), F18: Aspect (45), F19: Local mean depth (15), and F20: Eastness (15).

As illustrated in Fig. 7 and Table VIII, when the input features are the combination of multispectral and bathymetric features optimized by the ReliefF–mRMR method, the classification accuracies are ordered as follows: RF (94.85%)>XGBoost (93.38%)>SVM (89.52%)>KNN (88.60%). RF and XGBoost perform well independently of the input characteristics, with accuracies above 90%. RF is more accurate than XGBoost, mainly reflected in the fact that less sand is misclassified into coral reefs with the RF method. Continuously distributed algal ridges show a break in the XGBoost result map. For the reef crest, all models achieve satisfactory results, where the true samples are almost precisely predicted.

Compared with multispectral features alone, the multisource features yield a maximum increase of 3.31%. Greater variation occurs with bathymetric features, where the accuracies are 11.76%–17.28% lower than those achieved with multisource features. Using multispectral data alone yield better results than using bathymetric data alone, possibly because multispectral data are directly related to the substrate properties, while bathymetric data represent indirect constraint information. However, the bathymetric features are considered important in Fig. 6 because the calculated weight or contribution degree is specific to the features, which does not directly reflect the classification accuracy. Taking RF as an example, compared with those achieved with multispectral features, the accuracies of multisource features increase by up to 8.27% (UA) and 6.20% (PA), respectively. For bathymetric features, the accuracies of all classes exhibit noticeable decreases relative to those achieved with multisource features, with the largest changes in the sand (up to 32.87%) and coral fragments and gravel (up to 28.20%).

We then compare and statistically evaluate the classification performance among different feature selection methods (see Table IX). Regardless of the classifier, our proposed ReliefF–mRMR method consistently presents the highest accuracies, followed by ReliefF and no feature selection method. The largest discrepancy is seen with SVM, where the accuracy of ReliefF–mRMR–SVM is 19.30% and 30.70% higher than that of ReliefF–SVM and SVM, respectively. For other classifiers, the accuracies of ReliefF–mRMR are still 1.28%–2.75% and 2.75%–4.78% larger than those of ReliefF and the original feature set. ReliefF–mRMR achieves an improvement over VIF (of 7.35%) and FR (of 2.75%). PCA has poor performance, presenting 15.07%–21.69% lower accuracies than ReliefF–mRMR. The reason for this poor performance may be that the candidate features contain both bathymetric derivatives and the texture and spectral information of the multispectral image. Thus, the significant difference between these features is not conducive to being mapped to the new dimension by PCA.

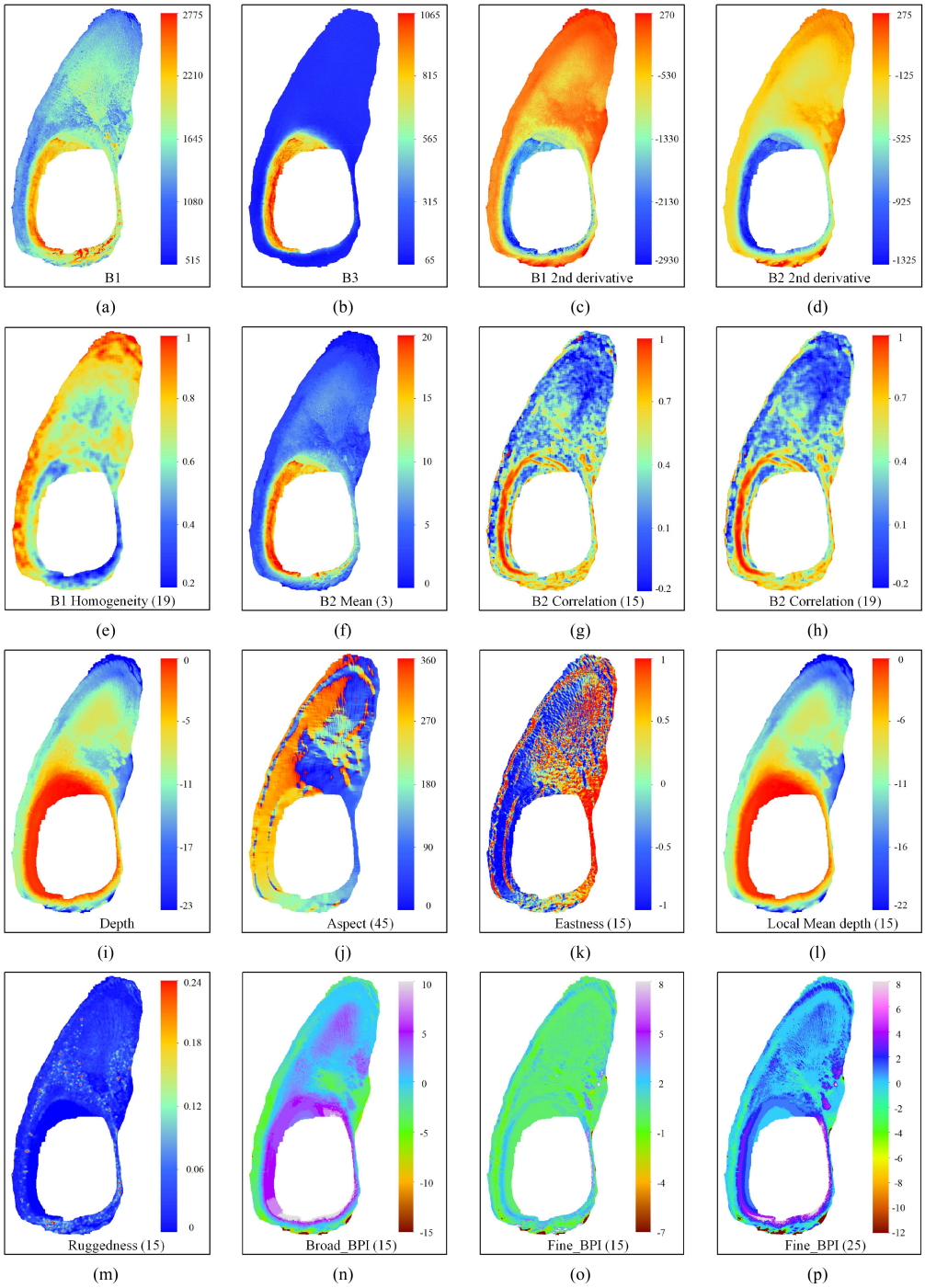

Fig. 5. Final 16 features for classification (the number in brackets means the scale of features). (a) B1. (b) B3. (c) B1 second derivative. (d) B2 second derivative. (e) B1 homogeneity (19). (f) B2 mean (3). (g) B2 correlation (15). (h) B2 correlation (19). (i) Depth. (j) Aspect (45). (k) Eastness (15). (l) Local mean depth (15). (m) Ruggedness (15). (n) Broad_BPI (15). (o) Fine_BPI (15). (p) Fine_BPI (25).

The classification methods are also visually evaluated by seafloor habitat maps (see Fig. 8). Regardless of the input variables, the prediction results given by the four supervised classification methods are generally consistent. Still, large differences remain between the perspectives of local details. When using multisource features, the map produced by RF is the most accurate representation of reality, followed by XGBoost. A small area of reefs exists between the coral sand and reef crest on the north side of the land. However, in the experimental results, some sand areas are undetected in the slight gaps between reef blocks. The classification map of bathymetric data shows that coral reefs are distributed in large aggregations; in reality, they are scattered throughout the coral sand. In addition, the area of the reef crest is larger than the actual area because the sand or coral reef is misclassified as a reef crest. We subsequently calculate the intermodel agreement based on

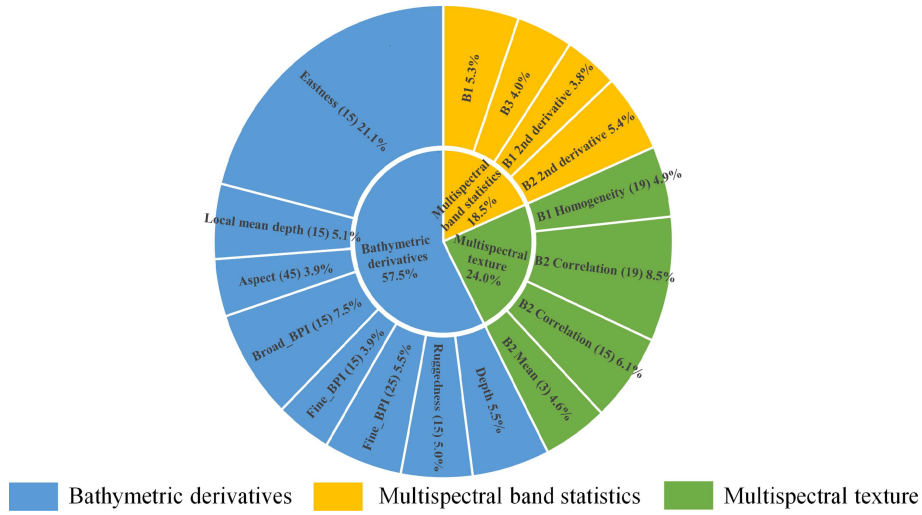

Fig. 6. Schematic of the weights of different features.

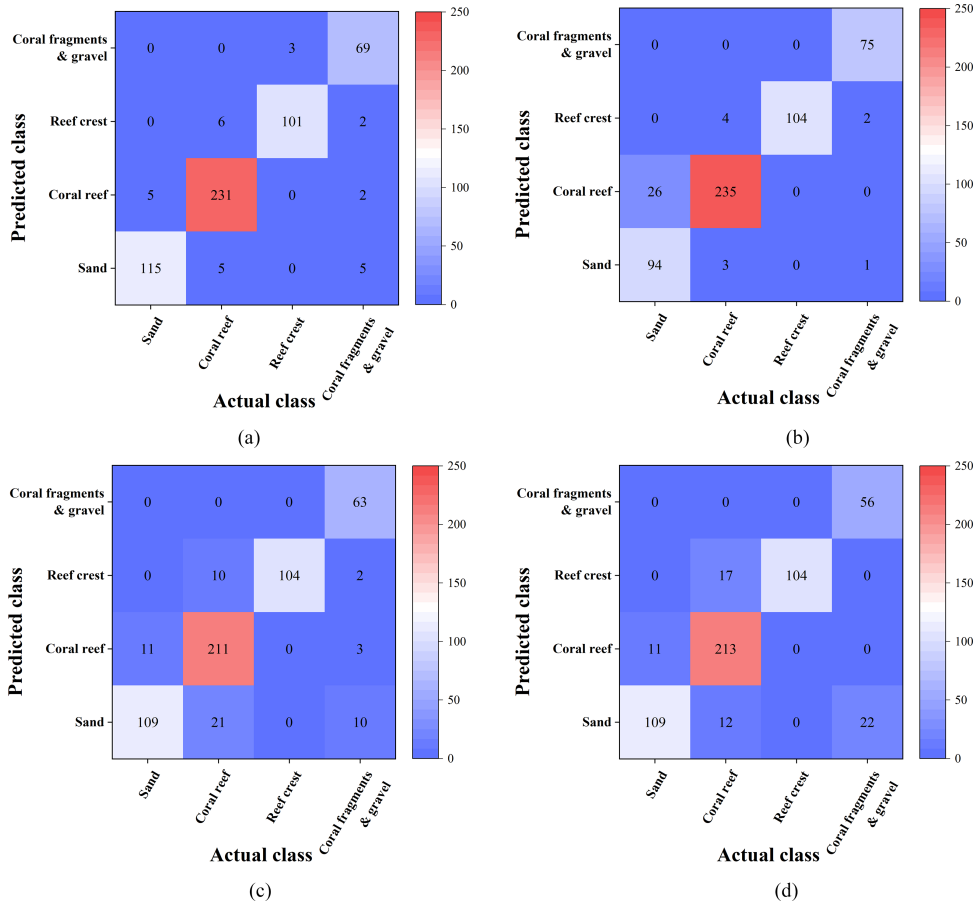

Fig. 7. Confusion matrices of different classifiers using our proposed method. (a) RF. (b) XGBoost. (c) SVM. (d) KNN.

the resulting map (see Table X). From the table, it can be concluded that the agreement between different classifiers is high. The agreement between RF and XGBoost ranks first at 93.34%, perhaps because both classifiers belong to ensemble learning.

V. Discussion

This article proposes a seafloor habitat mapping method combining optic and acoustic remote sensing features. Using the ReliefF–mRMR feature selection method, we select the

TABLE IX
COMPARISON OF CLASSIFICATION ACCURACIES UNDER DIFFERENT FEATURE SELECTION METHODS

Classifier	Feature selection	Number of bands	OA(%)	Kappa	*F*1-score
RF	None	158	91.91	0.883	0.918
	PCA	3	79.41	0.702	0.793
	FR	56	94.30	0.917	0.942
	VIF	40	88.60	0.832	0.882
	ReliefF	72	92.65	0.895	0.926
	ReliefF–mRMR	16	**94.85**	**0.926**	**0.948**
XGBoost	None	158	90.63	0.864	0.904
	PCA	3	75.18	0.641	0.751
	FR	56	92.46	0.890	0.923
	VIF	40	92.28	0.887	0.921
	ReliefF	72	92.10	0.886	0.921
	ReliefF–mRMR	16	93.38	0.904	0.932
SVM	None	158	58.82	0.312	0.516
	PCA	3	67.83	0.523	0.672
	FR	56	70.04	0.525	0.663
	VIF	40	69.85	0.531	0.671
	ReliefF	72	70.22	0.532	0.662
	ReliefF–mRMR	16	89.52	0.851	0.896
KNN	None	158	83.82	0.770	0.836
	PCA	3	73.53	0.610	0.730
	FR	56	85.85	0.796	0.854
	VIF	40	81.25	0.734	0.810
	ReliefF	72	85.85	0.798	0.855
	ReliefF–mRMR	16	88.60	0.838	0.886

*Bold numbers represent the highest accuracy in the same column.

TABLE X
INTERMODEL AGREEMENT (IN %), CALCULATED FROM THE RESULT MAPS

Classifier	RF	XGBoost	SVM	KNN
RF		93.34	83.67	83.77
XGBoost			85.22	84.41
SVM				89.14
KNN				

scales of features that best represent the processes of interest and ultimately obtain multisource multiscale features most favorable for classification. This method overcomes the problem that single-source data cannot completely cover the study area and have difficulty fully reflecting the substrate distribution characteristics. Based on the above results, several issues are further discussed in the following sections.

A. *Comparability of the Classification Results*

From the results of different classifiers, we can conclude that when the combination of multisource features is input, RF and XGBoost are both superior to SVM and KNN, in line with previous seafloor habitat classification studies [26], [44]. In comparison to ReliefF or no feature selection approach, using ReliefF–mRMR is identified with the highest accuracies. This may be because many irrelevant and redundant features negatively affect the classification when the feature size is large. The fact that RF and XGBoost use ensemble learning techniques, which combine multiple classifiers with more stable characteristics than a single classifier, may explain why the performance of these approaches is less impacted by feature selection. In contrast, SVM struggles to perform effectively with a high number of features because it has poor training properties on large data and is prone to being impacted by negative data [54].

Compared with the adjacent coral fragments and gravel, the proportion of reef crest samples correctly classified by RF is 8.66% larger. Sand tends to be distributed between coral reefs, and in RF, the classification accuracy of coral reefs is higher than that of sand for all the inputs. This may be because the distribution of sand is concentrated around the land and in the dense coral reef area in the north. The nature of sand in these two places differs somewhat and, thus, affects the classification accuracy.

We also compare the classification results of different feature sets after using the ReliefF–mRMR algorithm. Fig. 9 shows that the accuracies remain highest when the number of features is 20. Therefore, this article uses the ReliefF–mRMR algorithm to select 20 features and then remove features with high correlation coefficients to obtain the final 16 features for the classification task. When the number of features is less than 20, the accuracies of the classifiers exhibit upward trends as the number of features grows. Above 20 features, the accuracies of SVM tend to decrease significantly as the number of features increases, while other classifiers show fluctuations within a certain range.

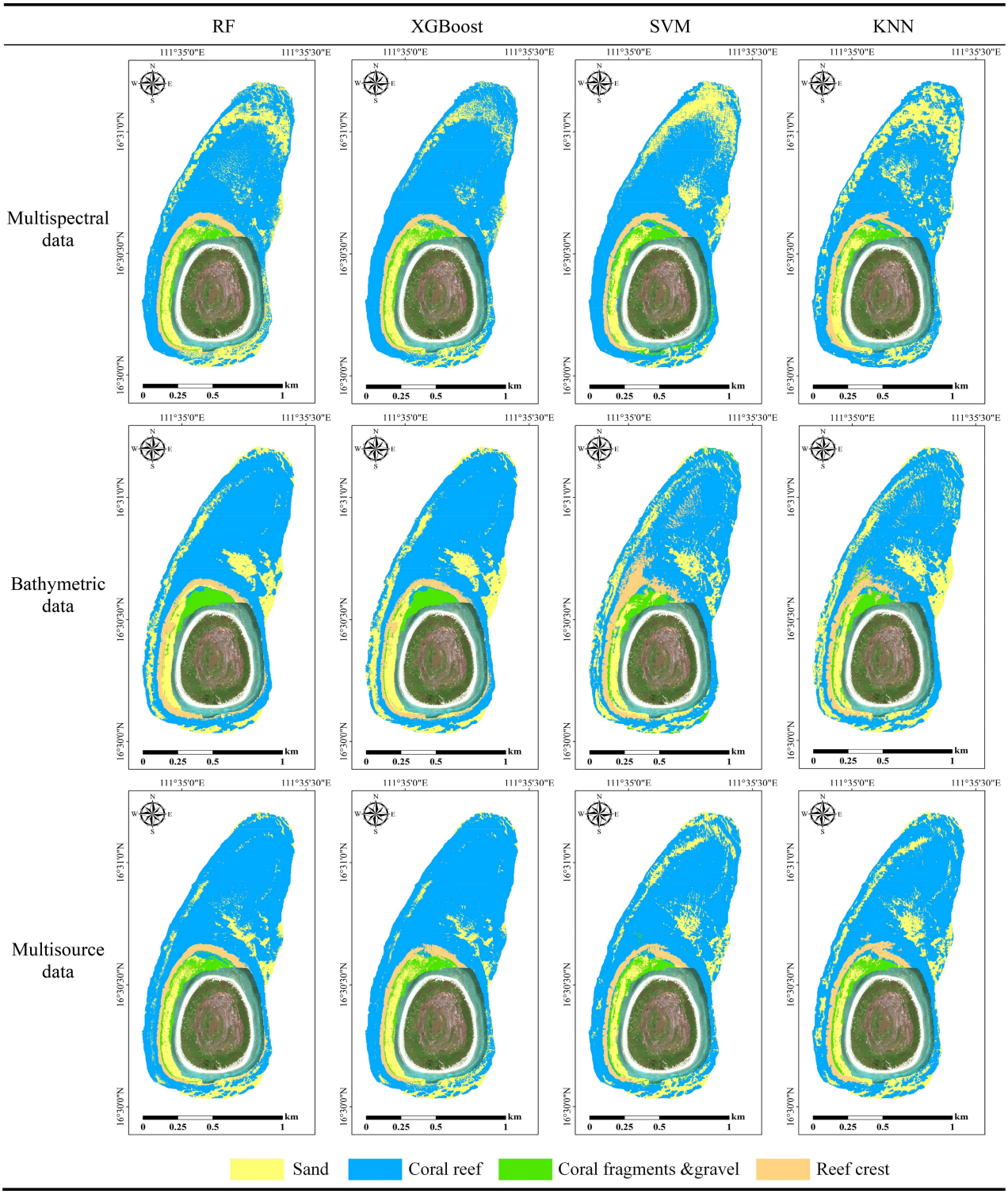

Fig. 8. Seafloor habitat maps of different data sources by multiple classifiers. The input data are the same in each row; the classification methods are consistent in each column.

B. Distribution of Topographic Features for Different Habitat Types

Topographic factors derived from bathymetric data are influenced by the structure and properties of the seafloor. For example, the slope and bathymetric position indices derived from bathymetric data represent the structural properties of the seafloor influenced by submarine wave energy and bottom currents; the topographic roughness reflects the spatial sensitivity of the seafloor substrates [14], [55]. These characteristics

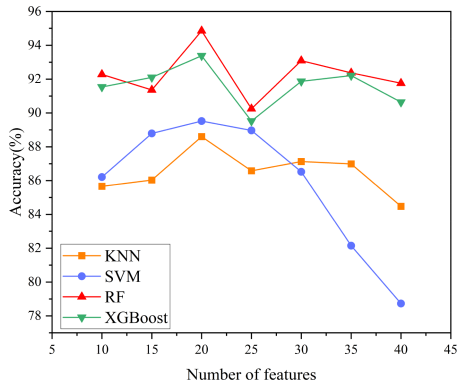

Fig. 9. Performance of different classifiers when the number of features increases (For display purposes, the horizontal coordinate refers to the number of features without correlation analysis; the actual result is after correlation analysis.).

of the bottom have significant impacts on how substrates are distributed. Therefore, these topographic factors are related to benthic substrate types. We use boxplots to visually depict the effects of topographic factors on the distribution of substrates (see Fig. 10).

As shown in Fig. 10, the selected topographic features clearly discriminate between various substrates, indicating that these features may contribute to the classification process. Both reef crest and coral fragments are distributed in shallower areas with larger slopes. In contrast, sand and coral reefs are widely distributed in deeper areas, covering a large range of slopes. The fact that Fine_BPI (15) and Fine_BPI (25) have different values highlights the importance of choosing the proper scale of features. Although several studies have shown relationships between topographic parameters and substrate type [14], [42], additional research and in-depth analysis are needed.

C. Coral Coverage Estimation

To better characterize the geomorphic formation process of the seafloor, we develop a coral reef geomorphic unit system based on substrate classification maps. This system is based on many previous studies [56], [57], [58], [59]. The system considers the oceanic processes in the formation process of coral reef geomorphology and dynamic factors, and coral coverage is taken into account in the development of the classification system. This system is able to direct the conservation and cultivation of coral reefs in addition to providing technical support for the dynamic monitoring of coral reefs. Table XI presents the coral reef geomorphic unit system in this study area, including distribution characteristics, multispectral images, and field photos. The study area includes the shallow slope of the fore reef, reef crest, reef-clumping area, and reef-depositional area. We cut, merge, and reclassify the RF result map of multisource features in Section IV-B according to expert knowledge and visual interpretation, and finally produce the coral reef geomorphic unit map of Ganquan Island (see Fig. 11).

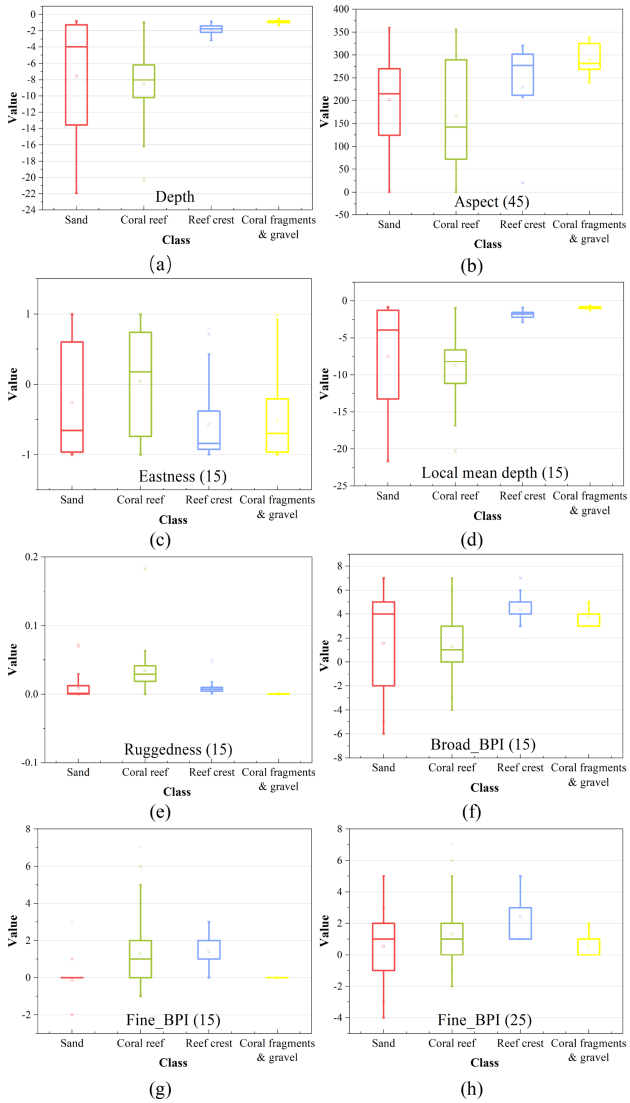

Fig. 10. Boxplots of the habitat distribution of topographic factors for different classes. (a) Depth. (b) Aspect (45). (c) Eastness (15). (d) Local mean depth (15). (e) Ruggedness (15). (f) Broad_BPI (15). (g) Fine_BPI (15). (h) Fine_BPI (25).

Fig. 11 shows that a tiny reef-clumping area with abundant corals is situated in the northern section of the nearshore reef-depositional area, primarily distributed close to the land. A narrow transitional zone, known as the reef crest, exists outside the reef-depositional area. Outside the reef crest, the shallow slope of the fore reef is dominated by large coral reefs, whose surrounding seafloor is primarily covered by sand. The average coral coverage D in the study area can be estimated using the following equation by measuring the coral coverage of various geomorphological units [58] (see Table XII):

$$D = \sum \frac{S_i}{S} \times d_i \tag{5}$$

where S_i is the area of each geomorphic unit, d_i is the estimated coral coverage of each geomorphic unit, and S is the total area

TABLE XI
CORAL REEF GEOMORPHIC UNIT SYSTEM IN THE STUDY AREA

Geomorphic unit	Description	Multispectral image	Field photo
Shallow slope of fore reef	The area where the inner reef edge is covered with a large number of healthy living corals. The coral grows to the seaward side and expands the reef flat with the low-tide surface as the upper limit.		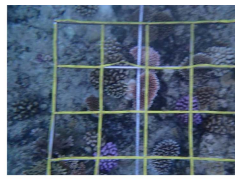
Reef crest	A smooth bump covered by algae. Primarily distributed in the outer margin of the reef flat, exposed from the sea surface at low tide. With strong hydrodynamic action, grooves exist in a part of the area. Only sporadic corals grow here.		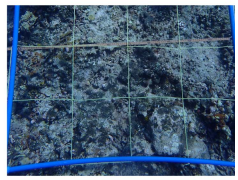
Reef-clumping area	Hard substrate composed mainly of healthy live corals and some biological debris, where hydrodynamic action is weak, with a large number of well-developed corals on it.	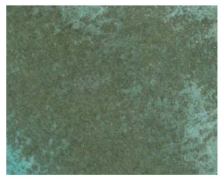	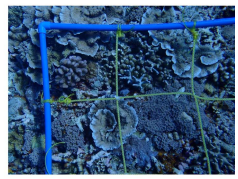
Reef-depositional area	It is in the inner part of the reef edge, mainly composed of coral sand and sparse corals. The inner part of the reef margin is weakly hydrodynamic, where sedimentation is the main effect.		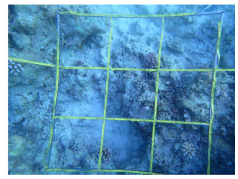

TABLE XII
CORAL REEF GEOMORPHIC UNIT SYSTEM IN THE STUDY AREA

Class	Shallow slope of fore reef	Reef crest	Reef-clumping area	Reef-depositional area
Area(km^2)	0.93	0.11	0.01	0.06
Coral coverage	80%–90%	0%	80%–90%	30%–40%

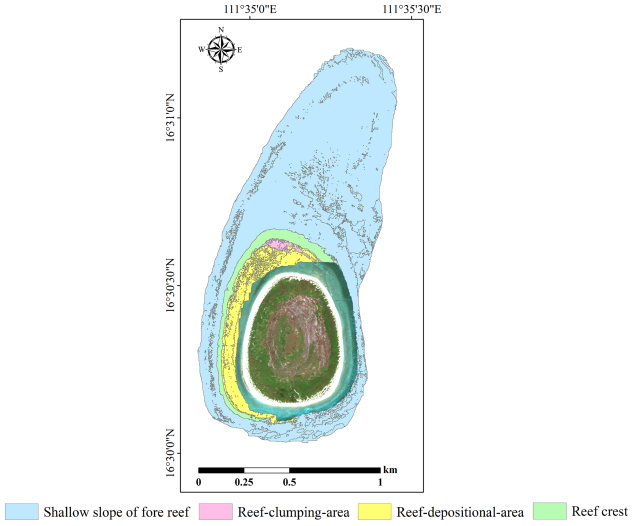

Fig. 11. Classification map of coral reef geomorphic units of Ganquan Island.

TABLE XIII
MODEL EVALUATION RESULTS WITH DIFFERENT INPUTS ON WUZHIZHOU ISLAND

Model	Feature combination	OA (%)	Kappa	*F*1-score
RF	Input1	78.36	0.65	0.78
	Input2	66.43	0.46	0.65
	Input3	82.26	0.71	0.82
XGBoost	Input1	73.85	0.57	0.74
	Input2	69.94	0.51	0.68
	Input3	77.86	0.64	0.78
SVM	Input1	67.94	0.48	0.67
	Input2	54.00	0.25	0.48
	Input3	70.74	0.51	0.70
KNN	Input1	78.56	0.64	0.79
	Input2	74.85	0.60	0.73
	Input3	**85.87**	**0.77**	**0.86**

* Input1, Input2, and Input3 represent the multispectral data only, bathymetric data only, and multisource data, respectively. The bold numbers represent the highest accuracy in the same column.

TABLE XIV
COMPARISON OF CLASSIFICATION ACCURACIES UNDER DIFFERENT FEATURE SELECTION METHODS ON WUZHIZHOU ISLAND

Classifier	Feature selection	Number of bands	OA(%)	Kappa	*F*1-score
RF	None	166	68.84	0.49	0.69
	PCA	13	79.75	0.67	0.80
	FR	59	75.35	0.60	0.75
	VIF	52	71.84	0.53	0.72
	ReliefF	102	69.14	0.50	0.69
	ReliefF–mRMR	14	82.26	0.71	0.82
XGBoost	None	166	63.93	0.42	0.64
	PCA	13	78.66	0.64	0.78
	FR	59	63.73	0.41	0.63
	VIF	52	46.99	0.12	0.48
	ReliefF	102	63.83	0.41	0.63
	ReliefF–mRMR	14	77.86	0.64	0.78
SVM	None	166	54.81	0.19	0.46
	PCA	13	52.00	0.21	0.45
	FR	59	54.71	0.19	0.46
	VIF	52	47.29	0.13	0.36
	ReliefF	102	54.81	0.19	0.46
	ReliefF–mRMR	14	70.74	0.51	0.70
KNN	None	166	80.76	0.69	0.81
	PCA	13	78.36	0.65	0.78
	FR	59	85.67	0.77	0.86
	VIF	52	77.05	0.63	0.77
	ReliefF	102	81.96	0.70	0.82
	ReliefF–mRMR	14	**85.87**	**0.77**	**0.86**

* Bold numbers represent the highest accuracy in the same column.

of the study area. The average coral coverage in the study area calculated by (5) is 70.85%–80.33%.

D. Wuzhizhou Island Application of the Proposed Method

We also assess the classification performance of Wuzhizhou Island. Tables XIII and XIV present the results of different inputs and different feature selection methods, respectively. When the input data are multisource features, all four classifiers perform best, with accuracies at most 7.31% and 16.74% higher than multispectral data only and bathymetric data only, respectively. KNN achieves the highest accuracy (85.87%), followed by RF (82.26%). The results of different feature selection methods also show that our proposed ReliefF–mRMR method presents the highest accuracies, with an improvement of 5.11%–15.93% over the no-selection method. Other feature selection methods achieve less improvement, some even inferior to the original input. The above experiments demonstrate the effectiveness of our proposed method in different regions.

E. Limitations

The MBES backscatter intensity, which directly reflects the diversity of various substrate types on the seafloor, is a common piece of information employed in multibeam seafloor habitat classification. However, the survey did not obtain high-quality backscatter intensity data due to disruptive echoes from the reefs. Therefore, our experiment only employs bathymetric features of multibeam acoustic data. In the future, incorporating backscatter intensity data, as well as the texture and statistics of backscatter to candidate features, might be beneficial for seabed mapping. Additionally, we will conduct more studies that include different times, water temperatures, or water qualities.

VI. CONCLUSION

This article proposes a supervised classification approach that employs multiscale optics and acoustics data fusion for coastal seafloor habitats. In nearshore coastal areas, single-source data yield images with noise and limited coverage; the employment of multisource data was able to compensate for the limited characterization capability of single-source data. To remove redundant and irrelevant features, optimal features with appropriate scales were selected by ReliefF–mRMR, which improved the quality of the features input into the classifier. The joint classification achieved the best classification result, with accuracy up to 3.31% and 17.28% higher than that obtained by multispectral data and bathymetric data only, respectively. In addition, we found that ReliefF–mRMR achieved significant improvement over other feature selection methods. By calculating the coral coverage of each geomorphic unit, we estimated that the average coral coverage for the study area is 70.85%–80.33%. This research provides feasible suggestions for mapping coastal areas by multisource data with high precision and has important implications for monitoring coral reef health. As a part of our ongoing study, we intend to conduct more experiments in other nearshore coastal regions and integrate backscatter characteristics to further enhance the predictive capability for seafloor habitats.

ACKNOWLEDGMENT

The authors would like to thank Prof. F. Yang at the Shandong University of Science and Technology and Prof. Q. Tang at

the First Institute of Oceanography, MNR, for providing the multibeam dataset and ground-truth samples.

REFERENCES

[1] C. J. Brown, S. J. Smith, P. Lawton, and J. T. Anderson, "Benthic habitat mapping: A review of progress towards improved understanding of the spatial ecology of the seafloor using acoustic techniques," *Estuarine, Coastal Shelf Sci.*, vol. 92, no. 3, pp. 502–520, May 2011, doi: 10.1016/j.ecss.2011.02.007.

[2] P. T. Harris and E. K. Baker, "GeoHab atlas of seafloor geomorphic features and benthic habitats—Synthesis and lessons learned," in *Seafloor Geomorphology as Benthic Habitat*, 2nd ed. Amsterdam, The Netherlands: Elsevier, 2020.

[3] T. C. Gaida, T. A. G. P. van Dijk, M. Snellen, T. Vermaas, C. Mesdag, and D. G. Simons, "Monitoring underwater nourishments using multibeam bathymetric and backscatter time series," *Coastal Eng.*, vol. 158, Jun. 2020, Art. no. 103666, doi: 10.1016/j.coastaleng.2020.103666.

[4] C. J. Brown, A. J. Hewer, D. S. Limpenny, K. M. Cooper, H. L. Rees, and W. J. Meadows, "Mapping seabed biotopes using sidescan sonar in regions of heterogeneous substrata: Case study east of the isle of wight, English channel," *Underwater Technol., Int. J. Soc. Underwater*, vol. 26, no. 1, pp. 27–36, Sep. 2004, doi: 10.3723/175605404783101558.

[5] C. B. L. da Silveira, G. M. R. Strenzel, M. Maida, A. L. B. Gaspar, and B. P. Ferreira, "Coral reef mapping with remote sensing and machine learning: A nurture and nature analysis in marine protected areas," *Remote Sens.*, vol. 13, no. 15, Jul. 2021, Art. no. 2907, doi: 10.3390/rs13152907.

[6] Y. Dong, Y. Liu, C. Hu, and B. Xu, "Coral reef geomorphology of the Spratly Islands: A simple method based on time-series of Landsat-8 multiband inundation maps," *ISPRS J. Photogramm. Remote Sens.*, vol. 157, pp. 137–154, Nov. 2019, doi: 10.1016/j.isprsjprs.2019.09.011.

[7] S. Andréfouët and O. Bionaz, "Lessons from a global remote sensing mapping project: A review of the impact of the millennium coral reef mapping project for science and management," *Sci. Total Environ.*, vol. 776, Jul. 2021, Art. no. 145987, doi: 10.1016/j.scitotenv.2021.145987.

[8] H. Su, H. Liu, L. Wang, A. M. Filippi, W. D. Heyman, and R. A. Beck, "Geographically adaptive inversion model for improving bathymetric retrieval from satellite multispectral imagery," *IEEE Trans. Geosci. Remote Sens.*, vol. 52, no. 1, pp. 465–476, Jan. 2014, doi: 10.1109/TGRS.2013.2241772.

[9] K. Aleksandra, M. Fantina, S. Marco, C. Ferrarin, and M. G. Giacomo, "Assessment of submerged aquatic vegetation abundance using multibeam sonar in very shallow and dynamic environment: The Lagoon of Venice (Italy) case study," in *Proc. IEEE/OES Acoust. Underwater Geosci. Symp. (RIO Acoust.)*, Rio de Janeiro, Brazil, 2015, pp. 1–7.

[10] M. Khomsin, D. G. Pratomo, and Suntoyo, "The development of seabed sediment mapping methods: The opportunity application in the coastal waters," *IOP Conf. Ser., Earth Environ. Sci.*, vol. 731, 2021, Art. no. 012039.

[11] G. Montereale Gavazzi, D. A. Kapasakali, F. Kerchof, S. Deleu, S. Degraer, and V. van Lancker, "Subtidal natural hard substrate quantitative habitat mapping: Interlinking underwater acoustics and optical imagery with machine learning," *Remote Sens.*, vol. 13, no. 22, Nov. 2021, Art. no. 4608, doi: 10.3390/rs13224608.

[12] S. Innangi et al., "Seabed mapping in the Pelagie islands marine protected area (Sicily channel, southern Mediterranean) using remote sensing object based image analysis (RSOBIA)," *Mar. Geophysical Res.*, vol. 40, no. 3, pp. 333–355, Oct. 2019, doi: 10.1007/s11001-018-9371-6.

[13] M. Diesing, P. J. Mitchell, E. O'Keeffe, G. O. A. M. Gavazzi, and T. L. Bas, "Limitations of predicting substrate classes on a sedimentary complex but morphologically simple seabed," *Remote Sens.*, vol. 12, no. 20, Oct. 2020, Art. no. 3398, doi: 10.3390/rs12203398.

[14] T. Pillay, H. C. Cawthra, and A. T. Lombard, "Characterisation of seafloor substrate using advanced processing of multibeam bathymetry, backscatter, and sidescan sonar in Table Bay, South Africa," *Mar. Geol.*, vol. 429, Nov. 2020, Art. no. 106332, doi: 10.1016/j.margeo.2020.106332.

[15] L. Koop, M. Snellen, and D. G. Simons, "An object-based image analysis approach using bathymetry and bathymetric derivatives to classify the seafloor," *Geosciences*, vol. 11, no. 2, Apr. 2021, Art. no. 45, doi: 10.3390/geosciences11020045.

[16] K. Zhang, Q. Li, H. Zhu, F. Yang, and Z. Wu, "Acoustic deep-sea seafloor characterization accounting for heterogeneity effect," *IEEE Trans. Geosci. Remote Sens.*, vol. 58, no. 5, pp. 3034–3042, May 2020, doi: 10.1109/TGRS.2019.2946986.

[17] A. Zelada Leon, V. A. I. Huvenne, N. M. A. Benoist, M. Ferguson, B. J. Bett, and R. B. Wynn, "Assessing the repeatability of automated seafloor classification algorithms, with application in marine protected area monitoring," *Remote Sens.*, vol. 12, no. 10, May 2020, Art. no. 1572, doi: 10.3390/rs12101572.

[18] H. M. Tulldahl, P. Philipson, H. Kautsky, and S. A. Wikström, "Sea floor classification with satellite data and airborne lidar bathymetry," *Proc. SPIE*, vol. 8724, pp. 100–115, 2013.

[19] M. Prampolini et al., "Benthic habitat map of the southern Adriatic Sea (Mediterranean Sea) from object-based image analysis of multi-source acoustic backscatter data," *Remote Sens.*, vol. 13, no. 15, Jul. 2021, Art. no. 2913, doi: 10.3390/rs13152913.

[20] M. Wang, Z. Wu, F. Yang, Y. Ma, X. H. Wang, and D. Zhao, "Multifeature extraction and seafloor classification combining LiDAR and MBES data around Yuanzhi Island in the South China Sea," *Sensors*, vol. 18, no. 11, Nov. 2018, Art. no. 3828, doi: https://doi.org/10.3390/s18113828.

[21] K. Zhang, F. Yang, H. Zhang, D. Su, and Q. Li, "Morphological characterization of coral reefs by combining lidar and MBES data: A case study from Yuanzhi Island, South China Sea," *J. Geophys. Res., Oceans*, vol. 122, no. 6, pp. 4779–4790, May 2017, doi: 10.1002/2016JC012507.

[22] K. Ismail, V. A. I. Huvenne, and D. G. Masson, "Objective automated classification technique for marine landscape mapping in submarine canyons," *Mar. Geol.*, vol. 362, pp. 17–32, Apr. 2015, doi: 10.1016/j.margeo.2015.01.006.

[23] M. Diesing, P. Mitchell, and D. Stephens, "Image-based seabed classification: What can we learn from terrestrial remote sensing?," *ICES J. Mar. Sci.*, vol. 73, no. 10, pp. 2425–2441, Nov. 2016, doi: 10.1093/icesjms/fsw118.

[24] X. Cui, F. Yang, X. Wang, B. Ai, Y. Luo, and D. Ma, "Deep learning model for seabed sediment classification based on fuzzy ranking feature optimization," *Mar. Geol.*, vol. 432, Feb. 2021, Art. no. 106390, doi: 10.1016/j.margeo.2020.106390.

[25] X. Ji, B. Yang, and Q. Tang, "Seabed sediment classification using multibeam backscatter data based on the selecting optimal random forest model," *Appl. Acoust.*, vol. 167, Oct. 2020, Art. no. 107387, doi: 10.1016/j.apacoust.2020.107387.

[26] D. Stephens and M. Diesing, "A comparison of supervised classification methods for the prediction of substrate type using multibeam acoustic and legacy grain-size data," *PLoS One*, vol. 9, no. 4, Apr. 2014, Art. no. e93950, doi: 10.1371/journal.pone.0093950.

[27] D. Su, F. Yang, Y. Ma, K. Zhang, J. Huang, and M. Wang, "Classification of coral reefs in the South China sea by combining airborne LiDAR bathymetry bottom waveforms and bathymetric features," *IEEE Trans. Geosci. Remote Sens.*, vol. 57, no. 2, pp. 815–828, Feb. 2019, doi: 10.1109/TGRS.2018.2860931.

[28] U. Bradter, W. E. Kunin, J. D. Altringham, T. J. Thom, and T. G. Benton, "Identifying appropriate spatial scales of predictors in species distribution models with the random forest algorithm," *Methods Ecol. Evol.*, vol. 4, no. 2, pp. 167–174, Feb. 2013, doi: 10.1111/j.2041-210x.2012.00253.x.

[29] B. Misiuk, V. Lecours, and T. Bell, "A multiscale approach to mapping seabed sediments," *PLoS One*, vol. 13, no. 2, Feb. 2018, Art. no. e0193647, doi: 10.1371/journal.pone.0193647.

[30] J. A. Strong, A. Clements, H. Lillis, I. Galparsoro, T. Bildstein, and R. Pesch, "A review of the influence of marine habitat classification schemes on mapping studies: Inherent assumptions, influence on end products, and suggestions for future developments," *ICES J. Mar. Sci.*, vol. 76, no. 1, pp. 10–22, Jan./Feb. 2019, doi: 10.1093/icesjms/fsy161.

[31] M. Miyamoto, M. Kiyota, H. Murase, T. Nakamura, and T. Hayashibara, "Effects of bathymetric grid-cell sizes on habitat suitability analysis of cold-water Gorgonian corals on seamounts," *Mar. Geodesy*, vol. 40, no. 4, pp. 205–223, May 2017, doi: 10.1080/01490419.2017.1315543.

[32] H. Hu, C. Feng, X. Cui, K. Zhang, X. Bu, and F. Yang, "A sample enhancement method based on simple linear iterative clustering superpixel segmentation applied to multibeam seabed classification," *IEEE Trans. Geosci. Remote Sens.*, vol. 61, Feb. 2023, Art no. 4202115, doi: 10.1109/TGRS.2023.3247827.

[33] R. M. Haralick, K. Shanmugam, and I. H. Dinstein, "Textural features for image classification," *IEEE Trans. Syst., Man, Cybern.*, vol. SMC-3, no. 6, pp. 610–621, Nov. 1973, doi: 10.1109/TSMC.1973.4309314.

[34] V. Lucieer, N. A. Hill, N. S. Barrett, and S. Nichol, "Do marine substrates 'look' and 'sound' the same? Supervised classification of multibeam acoustic data using autonomous underwater vehicle images," *Estuarine, Coastal Shelf Sci.*, vol. 117, pp. 94–106, 2013, doi: 10.1016/j.ecss.2012.11.001.

[35] M. F. J. Wilson, B. O'Connell, C. Brown, J. C. Guinan, and A. J. Grehan, "Multiscale terrain analysis of multibeam bathymetry data for habitat mapping on the continental slope," *Mar. Geodesy*, vol. 30, no. 1/2, pp. 3–35, May 2007, doi: 10.1080/01490410701295962.

[36] G. Hughes, "On the mean accuracy of statistical pattern recognizers," *IEEE Trans. Inf. Theory*, vol. 14, no. 1, pp. 55–63, Jan. 1968, doi: 10.1109/TIT.1968.1054102.

[37] D. Stathakis and K. Perakis, "Feature evolution for classification of remotely sensed data," *IEEE Geosci. Remote Sens. Lett.*, vol. 4, no. 3, pp. 354–358, Jul. 2007, doi: 10.1109/LGRS.2007.895285.
[38] A. Friedman, "Automated interpretation of benthic stereo imagery," Ph.D. dissertation, Faculty Eng. Inf. Technol., School Aerosp. Mech. Mechatron. Eng. Univ. Sydney, Sydney, Australia, 2013.
[39] Y. Zhang, C. Ding, and T. Li, "A two-stage gene selection algorithm by combining ReliefF and mRMR," in *Proc. IEEE 7th Int. Symp. Bioinf. Bioeng.*, Boston, MA, USA, 2007, pp. 164–171.
[40] L. Breiman, "Random forests," *Mach. Learn.*, vol. 45, pp. 5–32, 2001.
[41] M. Belgiu and L. Drăguţ, "Random forest in remote sensing: A review of applications and future directions," *ISPRS J. Photogramm. Remote Sens.*, vol. 114, pp. 24–31, Apr. 2016, doi: 10.1016/j.isprsjprs.2016.01.011.
[42] D. Ierodiaconou et al., "Combining pixel and object based image analysis of ultra-high resolution multibeam bathymetry and backscatter for habitat mapping in shallow marine waters," *Mar. Geophysical Res.*, vol. 39, pp. 271–288, Jan. 2018, doi: 10.1007/s11001-017-9338-z.
[43] T. Chen and C. Guestrin, "XGBoost: A scalable tree boosting system," in *Proc. 22nd ACM SIGKDD Int. Conf. Knowl. Discov. Data Mining*, San Francisco, CA, USA, 2016, pp. 785–794.
[44] F. Wang, J. Yu, Z. Liu, M. Kong, and Y. Wu, "Study on offshore seabed sediment classification based on particle size parameters using XGBoost algorithm," *Comput. Geosci.*, vol. 149, Apr. 2021, Art. no. 104713, doi: 10.1016/j.cageo.2021.104713.
[45] C. Cortes and V. Vapnik, "Support-vector networks," *Mach. Learn.*, vol. 20, no. 3, pp. 273–297, 1995.
[46] T. Kavzoglu and I. Colkesen, "A kernel functions analysis for support vector machines for land cover classification," *Int. J. Appl. Earth Observ. Geoinf.*, vol. 11, no. 5, pp. 352–359, Oct. 2009, doi: 10.1016/j.jag.2009.06.002.
[47] X. Cui, H. Liu, M. Fan, B. Ai, D. Ma, and F. Yang, "Seafloor habitat mapping using multibeam bathymetric and backscatter intensity multi-features SVM classification framework," *Appl. Acoust.*, vol. 174, Mar. 2021, Art. no. 107728, doi: 10.1016/j.apacoust.2020.107728.
[48] X. Ji, B. Yang, and Q. Tang, "Acoustic seabed classification based on multibeam echosounder backscatter data using the PSO-BP-AdaBoost algorithm: A case study from Jiaozhou Bay, China," *IEEE J. Ocean. Eng.*, vol. 46, no. 2, pp. 509–519, Apr. 2021, doi: 10.1109/JOE.2020.2989853.
[49] M. Diesing and D. Stephens, "A multi-model ensemble approach to seabed mapping," *J. Sea Res.*, vol. 100, pp. 62–69, Jun. 2015, doi: 10.1016/j.seares.2014.10.013.
[50] B. V. Dasarathy, "NN concepts and techniques," in *Nearest Neighbor (NN) Norms: NN Pattern Classification Techniques*. Washington, DC, USA: IEEE Computer Society Press, 1991.
[51] R. G. Congalton, "A review of assessing the accuracy of classifications of remotely sensed data," *Remote Sens. Environ.*, vol. 37, no. 1, pp. 35–46, Jul. 1991, doi: 10.1016/0034-4257(91)90048-B.
[52] J. Cohen, "A coefficient of agreement for nominal scales," *Educ. Psychol. Meas.*, vol. 20, no. 1, pp. 37–46, Apr. 1960, doi: 10.1177/001316446002000104.
[53] N. Chinchor and B. Sundheim, "MUC-5 evaluation metrics," in *Proc. 5th Conf. Message Understanding*, Baltimore, MD, USA, 1993, pp. 69–78.
[54] L. Demidova, E. Nikulchev, and Y. Sokolova, "Big data classification using the SVM classifiers with the modified particle swarm optimization and the SVM ensembles," *Int. J. Adv. Comput. Sci. Appl.*, vol. 7, no. 5, pp. 294–312, 2016.
[55] B. M. Costa and T. A. Battista, "The semi-automated classification of acoustic imagery for characterizing coral reef ecosystems," *Int. J. Remote Sens.*, vol. 34, no. 18, pp. 6389–6422, Feb. 2013, doi: 10.1080/01431161.2013.800661.
[56] J. Leon and C. D. Woodroffe, "Improving the synoptic mapping of coral reef geomorphology using object-based image analysis," *Int. J. Geograph. Inf. Sci.*, vol. 25, no. 6, pp. 949–969, Jul. 2011, doi: 10.1080/13658816.2010.513980.
[57] S. R. Phinn, C. M. Roelfsema, and P. J. Mumby, "Multi-scale, object-based image analysis for mapping geomorphic and ecological zones on coral reefs," *Int. J. Remote Sens.*, vol. 33, no. 12, pp. 3768–3797, Dec. 2012, doi: 10.1080/01431161.2011.633122.
[58] J. Dong, G. Ren, Y. Hu, J. Pang, and Y. Ma, "Construction and classification of coral reef geomorphic unit system based on high-resolution remote sensing: Using 8-band worldview-2 image as an example," *J. Trop. Oceanogr.*, vol. 39, no. 4. pp. 116–129, 2020, doi: 10.11978/2019100.
[59] J. Wan and Y. Ma, "Multi-scale spectral-spatial remote sensing classification of coral reef habitats using CNN-SVM," *J. Coastal Res.*, vol. 102, pp. 11–20, Dec. 2020, doi: 10.2112/SI102-002.1.

Jiaxin Wan received the M.S. degree in surveying and mapping engineering from the College of Oceanography and Space Informatics, China University of Petroleum (East China), Qingdao, China, in 2020. She is currently working toward the Ph.D. degree in underwater acoustic engineering with the College of Underwater Acoustic Engineering, Harbin Engineering University, Harbin, China.

Her research interests include marine technology, seafloor habitats classification, and multibeam echo sounding system data processing.

Zhiliang Qin received the Ph.D. degree in marine geology from the Institute of Oceanology, Chinese Academy of Sciences, Qingdao, China, in 2012.

He has been a Professor with the College of Underwater Acoustic Engineering, Harbin Engineering University, Harbin, China, since 2017. He is the Head of the scientific research team of Acoustic Oceanography. His research interests include the theory and application of acoustic oceanography, sedimentary dynamics, and marine technology.

Xiaodong Cui received the Ph.D. degree in geodesy and geomatics from the Shandong University of Science and Technology, Qingdao, China, in 2021.

He is currently a Lecturer with the College of Geomatics, Shandong University of Science and Technology, Qingdao, China. His research interests include marine surveys, multibeam echo sounding system data processing, and acoustic seabed classification system.

Muhammad Yasir received the B.S. degree in geology from the University of Peshawar, Peshawar, Pakistan, in 2018, and the master's degree in geological engineering in 2021 from the China University of Petroleum, Qingdao, China, where he is currently working toward the Ph.D. degree in marine resources and information engineering with the College of Oceanography and Space Informatics.

He has several research publications in well-reputed international journals as a first, and coauthors. His research interests include computer vision and remote sensing image object detection, remote sensing image processing techniques, and systematic literature review.

Benjun Ma received the Ph.D. degree in marine geology from the Institute of Oceanology, Chinese Academy of Sciences, Qingdao, China, in 2017.

He has been an Associate Professor with the College of Underwater Acoustic Engineering, Harbin Engineering University, Harbin, China, since 2018. His research interests include acoustic oceanography, seismic interpretation, seismic inversion, and marine sedimentology.